Final Report

Application of Image Restoration Technique in Flow Scalar Imaging Experiment

Guanghua Wang

Center for Aeromechanics Research

Department of Aerospace Engineering and Engineering Mechanics

The University of Texas at Austin

Austin, Texas 78712-1085

Abstract

Scalar imaging techniques are widely used in fluid mechanics, but the effects of imaging system blur on the measured scalar gradients are often inadequately considered. Depending on the flow condition and imaging system used, the blurring can cause unacceptable errors in gradient related measurements, which are much larger than those for the scalar itself. Planar Laser-Induced Fluorescence (PLIF) images of turbulent jet fluid concentration were corrected for blur based on the Richardson-Lucy Expectation Maximization (R-L-EM) image restoration algorithm. This algorithm relies on the shot-noise limited nature of PLIF images and the measured Point Spread Function (PSF). The restored PLIF images show much higher peak dissipations and thinner fine-scale structures in the images, particularly when the structures are clustered.

1. Introduction

The spatial resolution of the optical system is very important for flow imaging experiments and it depends on many factors [1], e.g. pixel size of the detector array, depth of the collection optics and magnification. In many scalar imaging experiments, the resolution is usually quoted in terms of the area that each pixel images in the flow. For an ideal optical system or for an optical system used at high *f#* (*f# = f/D*, where *f* is the focal length and *D* is the diameter of the lens) and magnification is close to the design condition, resolution is nearly diffraction limited. However for low light level flow imaging experiments, such as Raman, Rayleigh and Planar Laser Induced Fluorescence (PLIF) imaging, fast (low *f#*) optics are commonly used. For these experiments, pixel size is not the only factor that limits the resolution. The imaging system blur should also be considered, since the image is the convolution of the Point Spread Function (PSF) with the irradiance distribution of the object. The smallest objects that can be resolved are related to the size and shape of the PSF. PSF also tends to progressively blur increasingly smaller structures. This is essentially a result of the system's inability to transfer contrast variations in the object to the image.

Depending on the flow condition and imaging system used, the PSF could be of the same order as the characteristic length scale of the scalar structures in the flow field, which may cause unacceptable error in the scalar measurement. To represent the TRUE scalar structure statistics, e.g. thickness, dissipation and Probability Density Function (PDF), it is necessary to restore the flow scalar experimental images. This project will introduce image restoration technique in flow scalar imaging applications and focus on how scalar measurements are affected. PLIF images of turbulent jet fluid concentration were corrected for blur based on the Richardson-Lucy Expectation Maximization (R-L-EM) image restoration algorithm. The shot-noise limited nature of PLIF images and the measured PSF are used to get reliable restoration.

2. Background

The general model [3-9] for a linear degradation caused by blurring and additive noise is

$$i(x,y) = h(x,y) * o(x,y) + n(x,y) \qquad (1)$$

where $i(x,y)$ is the blurred and noisy "observed image" corresponding to the observation of the "true image" $o(x,y)$, $h(x,y)$ is the blurring function or PSF of the imaging system, $*$ is the convolution operator, $n(x,y)$ denotes the additive noise such as the electronic or quantization noise involved in obtaining the image. In Fourier domain, the degradation is

$$I(u,v) = H(u,v) \cdot O(u,v) + N(u,v) \quad (2)$$

where $I(u,v)$, $H(u,v)$, $O(u,v)$ and $N(u,v)$ are the continuous Fourier transforms of $i(x,y)$, $h(x,y)$, $o(x,y)$ and $n(x,y)$ respectively and *u* and *v* are the spatial frequencies.

The purpose of restoration is to determine $o(x,y)$ knowing $i(x,y)$ and $h(x,y)$. This inverse problem has led to a large amount of work. Main difficulties are coming from the additive noise [3-9] and the PSF [7-9]. The modeling of blurring can be divided in two parts: blurring function and noise modeling. Some ideal PSF models are Gaussian, out-of-focus and linear motion blur [3]. In astronomy, data extracted from clear stars in observed image is used to fit a synthetic PSF function by weighted least square method [7, 8]. The PSF measurement techniques are also discussed in [1]. The diversity of algorithms [3-9] developed nowadays reflects different ways of recovering a "best" estimate of the "true image". Wiener and regularized filters are better for known PSF and additive noise [3, 4]. Some iterative restoration techniques [10], e.g. Expectation Maximization (EM) algorithms, work better for known PSF and unknown additive noise. Blind image restoration algorithms [5, 6] are more proper for unknown PSF and additive noise. Flow imaging experiments have a lot in common with astronomy observations. They both involve low light level imaging. In both cases images are degraded by imaging optical system and suffer from signal dependent noise (Poisson noise), CCD camera read-out noise and quantization noise. These physical similarities suggest that a better starting point in applying image restoration techniques in flow scalar image restoration is to consider those successful ones in astronomy.

3. Richardson-Lucy Expectation Maximization (R-L-EM) algorithm

The Richardson-Lucy algorithm ([11, 12]), also called the expectation maximization (EM) method, is an iterative technique used heavily for the restoration of astronomical images in the presence of Poisson

noise [7-9]. It attempts to maximize the likelihood of the restored image by using the Expectation Maximization (EM) algorithm. The EM approach constructs the conditional probability density [7, 10]

$$p(o \mid i) = p(i \mid o)\, p(o) / p(i) \tag{3}$$

where $p(i)$ and $p(o)$ are the probabilities of the observed image ***i*** and the true image ***o*** respectively. Here $p(i \mid o)$ is the probability distribution of observed image ***i*** if ***o*** were the true image. The Maximum Likelihood (ML) solution maximizes the density $p(i \mid o)$ over o

$$o_{ML} = \arg\max_{o} p(i \mid o) \tag{4}$$

where "argmax" means "the value that maximizes the function". For true image ***o*** with Poisson noise

$$p(i \mid o) = \prod_{x,y} e^{-(h*o)} \frac{(h*o)^i}{i!} \tag{5}$$

The maximum can be computed by setting the derivative of the logarithm to zero

$$\partial \ln p(i \mid o) / \partial o = 0 \tag{6}$$

The EM algorithm consists of two steps [11]: expectation step (E-step) and maximization step (M-step). These two steps are iterated until convergence. In practice, they are usually combined together to reduce the storage of results from E-step. Assuming the PSF is normalized to unity, a typical iteration is

$$o^{(k+1)}(x,y) = o^{(k)}(x,y)\left[\frac{i(x,y)}{h(x,y) * o^{(k)}(x,y)} * h^*(x,y) \right] \tag{7}$$

where $h^*(x,y) = h(-x,-y)$ and $o^{(k)}(x,y)$ is the estimate of the true image $o(x,y)$ after ***k*** iterations. The image $h(x,y) * o^{(k)}(x,y)$ is referred to as the re-blurred image [13].

Figure 1 is the flow chart of the basic iteration procedures of the R-L-EM algorithm [14] and it converges to the ML solution for Poisson statistics in the data. Constraints, e.g. non-negativity (estimate of the image must be positive), finite support (the object belongs to a given spatial domain), band-limited (the Fourier transform of the object belongs to a given frequency domain) and local and global conservation of flux at each iteration, can be incorporated in the basic iterative scheme.

Every iteration of the EM algorithm increases the likelihood function until a point of (local) maximum is reached. One way to suppress the noise amplification with increasing iterations is to use the

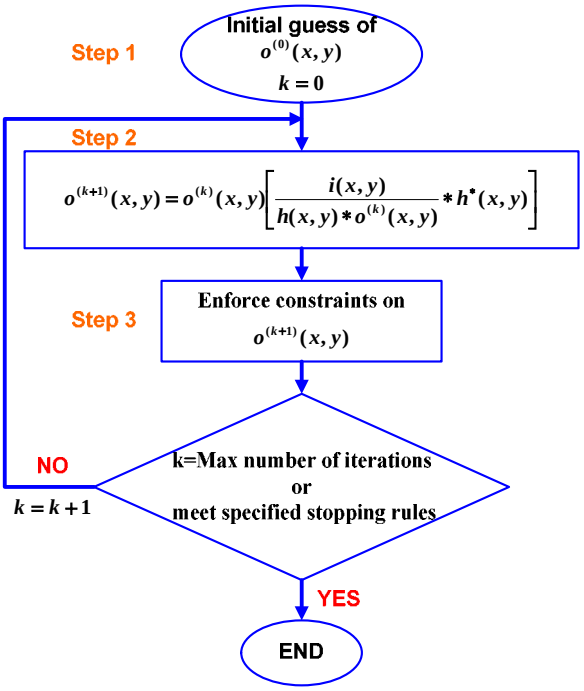

Fig. 1 Flow chart of the R-L-EM algorithm [14]

following iterative scheme

$$o^{(k+1)}(x,y) = f\left\{o^{(k+1)}(x,y)\right\} \qquad (8)$$

where $\boldsymbol{f}$ is the projection operator that enforces the set of constraints on $o^{(k+1)}(x,y)$ and some forms of $\boldsymbol{f}$ are given in [7-9]. In order to enforce constraints, the projection and back-projection operations can be performed using the Fast Fourier Transform (FFT). Each iteration needs one FFT in the projection step and one in the back-projection step depending on how many constraints are applied. Other computations are vector operations that have little impact on CPU time. Thus the R-L-EM algorithm is essentially an algorithm with two FFTs per iteration. The stopping rule is often based on the statistics of residual noise [4]

$$\text{Relative Error} = \frac{\left\|o^{(k+1)}(x,y)-o^{(k)}(x,y)\right\|}{\left\|o^{(k)}(x,y)\right\|} \le \varepsilon \qquad (9)$$

where ε is a small number. There are many modifications and improvements to overcome different drawbacks in the original R-L-EM algorithm, e.g. noise handling [7-9] and iteration acceleration (automatic acceleration [13]).

4. Simulation Results

PLIF is a well-developed technique and has been used extensively in studying non-reacting flows [1]. The acetone PLIF images used here are from "Condition 2" in [2] for a high Re jet flow and one image is shown in Figure 2. Here *i(x,y)* is the observed PLIF image corresponding to the jet fluid concentration field and is essentially shot-noise limited (Poisson noise) due to the high differential cross section (~10^{-24} cm^2/sr) and the large number of molecules in the cold jet flow. Scalar dissipation rate is an important quantity in turbulent scalar flow theory and modeling, which is defined as

$$\chi(x,y) = D\cdot\nabla i(x,y)\cdot\nabla i(x,y) \qquad (10)$$

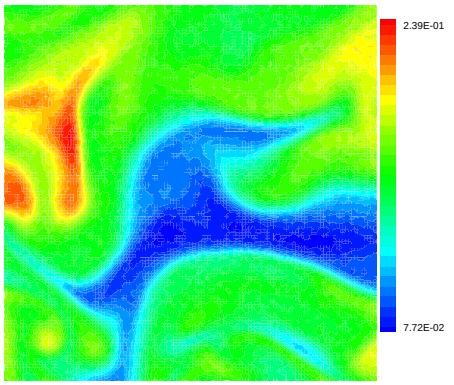

Fig. 2 Acetone PLIF image [2]

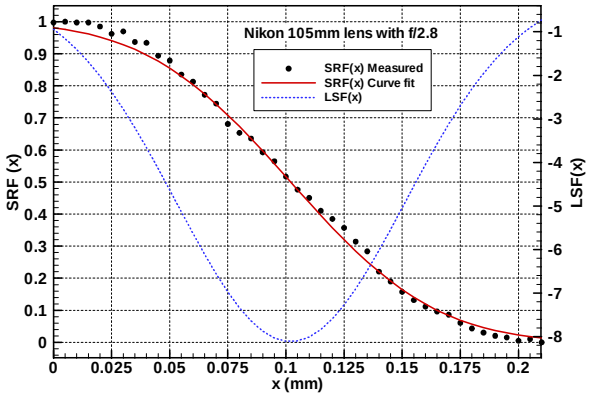

Fig. 3 Measured SRF and LSF for a Nikon lens f/2.8 [2]

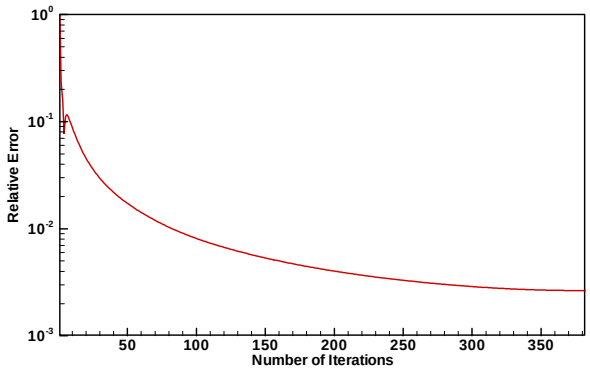

(a) Relative error vs. number of iterations

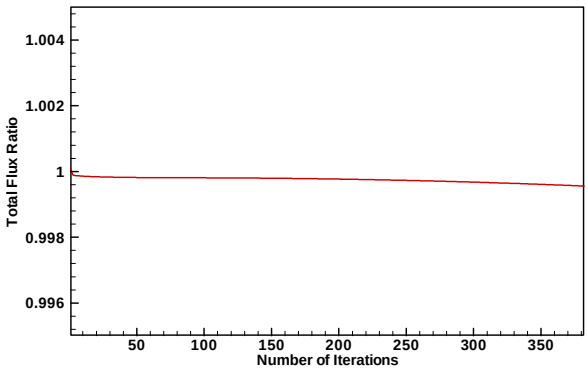

(b) Total flux ratio at each iteration

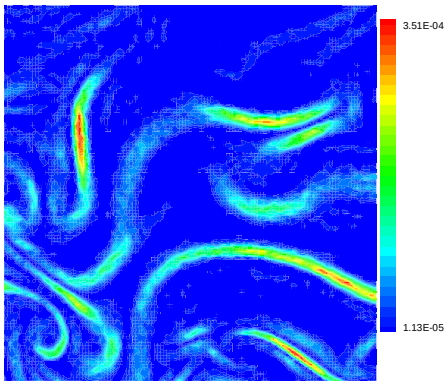

(c) Scalar dissipation field of Figure 2

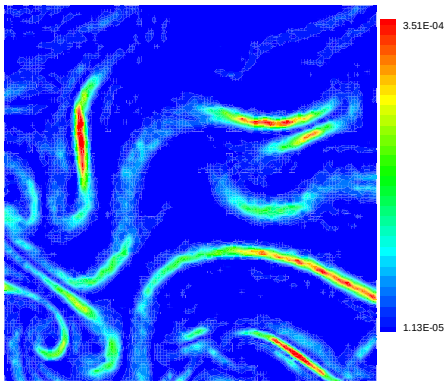

(d) Restored dissipation field

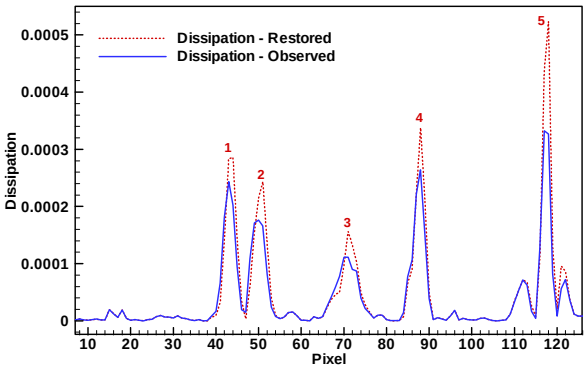

(e) Cross-cut profile of (d) at x=100 pixel

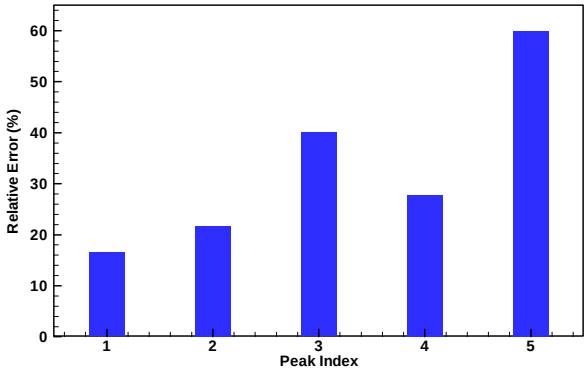

(f) Relative errors for the peak dissipation of (e)

Fig. 4 Restoration results of the R-L-EM algorithm for the acetone PLIF image in Figure 2

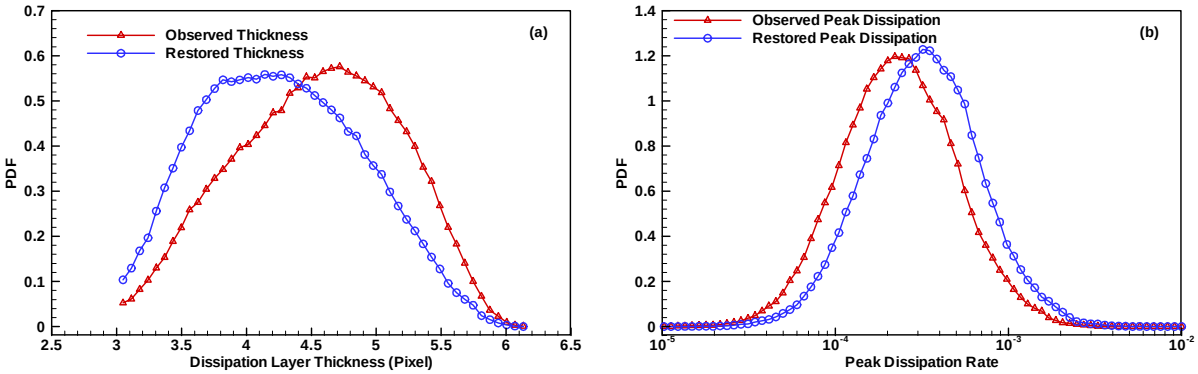

Fig. 5 PDF for (a) Dissipation layer thickness, (b) Peak dissipation rate

where D is the mass diffusivity and is set to one here to simplify the analysis. The 20% dissipation layer thickness is defined as twice the distance from the peak dissipation to where the dissipation falling to 20% of the peak value. It is obvious that any change in peak dissipation will also affect the layer thickness. The problem is to restore the true concentration *o* from the observed *i* and study the influences of image restoration on the scalar dissipation rate and dissipation layer thickness.

The PSF is measured by the scanning knife edge technique in [2]. The Step Response Function (SRF) is actually measured and differentiated to get the Line Spread Function (LSF). Figure 3 shows the measured SRF and LSF for a Nikon 105mm lens f/2.8 with a back-illuminated CCD camera (Cryocam S5 series). The PSF used here is constructed from the measured LSF by assuming an isotropic PSF. The iteration stops when the relative error is less than 0.002 or the maximum iteration number of 500 is reached. The relative error normally drops rapidly in the first few iterations and slows with the increasing restoration. Figure 4 (a) shows the path of the relative error from a 382-iteration R-L-EM restoration on a PLIF image in Figure 2.

The conservation of total flux is illustrated in Figure 4(b). The total flux ratio is defined as

$$\text{Total Flux Ratio} = \sum_{x,y} o^{(k+1)}(x,y) \Big/ \sum_{x,y} i(x,y) \qquad (11)$$

Maintaining the conservation of total flux is important for flow imaging application since the restoration should not alter the total number of photons detected.

The peak dissipation in the restored field is higher and the dissipation layer is thiner as comparing observed dissipation field in Figure 4(c) and the corresponding restored one in 4(d). The peak dissipation of the dissipation layer centerline is significantly reduced by the imaging system blur as shown in Figure

4(e), which are cross-cut profiles at x = 100 pixel from Figure 4(c) and 4(d). The relative errors between the observed and restored peak dissipation rate are shown in Figure 4(f) and typically 10% relative errors are observed. The maximum relative error occurs when the dissipation layers are thin and clustered together, which could be of the order of 60%, e.g. peak index 5 in Figure 4(e) and 4(f).

The PDF of the dissipation layer thickness and peak dissipation rate, as shown in Figure 5, are also generated by counting 3000 PLIF images. The restored layer thickness PDF shifts left comparing with that of the observed PDF, which means that the restored dissipation layers are usually thinner than those observed layers. The restored peak dissipation PDF shifts right with respect to that of the observed PDF, which tells that the restored peak dissipation rates are usually higher than those observed peak dissipation rates. This clearly shows that imaging system blur reduces the peak dissipation rate and broads the dissipation layer. By the R-L-EM image restoration algorithm, to some extend, the resolution is improved (we can measure thinner layers) and peak dissipation rate measurement accuracy is improved.

5. Conclusions and future work

Planar Laser-Induced Fluorescence (PLIF) images of turbulent jet fluid concentration were corrected for blur based on the Richardson-Lucy Expectation Maximization (R-L-EM) image restoration algorithm. This algorithm is most cognizant of the physical constraints on the PLIF images (shot-noise limited) and the measured PSF by the scanning knife-edge technique. The restored PLIF images show much higher peak dissipation and thinner fine-scale structures in the images, particularly when the structures are clustered. This is further verified by the right-shifting of the peak dissipation PDF and the left-shifting of the dissipation layer thickness PDF. These results illustrate the potential of the R-L-EM algorithm to improve the flow scalar imaging resolution and gradient related measurement accuracy.

For most flow scalar imaging experiments, sequence short exposure of scalar images is usually recorded and multi-channel restoration technique can be used to get more reliable restorations [15], especially when the PSF is poorly known or unknown. Multi-scale restoration techniques are also developed to restore astronomy observation images, e.g. wavelet-Lucy algorithm [7], which has a better noise handling capability.

Reference

1. N. T. Clemens, “Flow Imaging”, in “*Encyclopedia of Imaging Science and Technology*”, Editor: J.P. Hornak, John Wiley and Sons, New York, 2002.
2. M. S. Tsurikov, “Experimental Investigation of the Fine Scale Structure in Turbulent Gas-Phase Jet Flows”, PhD dissertation, The University of Texas at Austin, 2002.
3. R. L. Lagendijk and J. Biemond, “Basic Methods for Image Restoration and Identification”, in “*Handbook of image and video processing*”, Editor: Al Bovik, Academic Press, San Diego, CA, 2000.
4. V. M. R. Banham and A. K. Katsaggelos, “Digital Image Restoration”, *IEEE Signal Processing Magazine*, vol. 14, no. 2, pp. 24-41, Mar.1997.
5. T. D. Kundur and D. Hatzinakos, “Blind Image Deconvolution”, *IEEE Signal Processing Magazine*, vol. 13, no. 3, pp. 43-64, May 1996.
6. T. D. Kundur and D. Hatzinakos, “Blind Image Deconvolution Revisted”, *IEEE Signal Processing Magazine*, vol. 13, no. 6, pp. 61-63, Nov. 1996.
7. J. Starck, E. Pantin and F. Murtagh, “Deconvolution in Astronomy: A Review”, *Publications of the Astronomical Society of the Pacific*, vol. 114, pp. 1051-1069, Oct. 2002.
8. R. Molina, J. Nunez, F. J. Cortijo and J. Mateos, “Image Restoration in Astronomy: A Bayesian Perspective”, *IEEE Signal Processing Magazine*, vol. 18, no. 2, pp.11-29, Mar. 2001.
9. R. J. Hanisch, R. L. White and R. L. Gilliland, “Deconvolutions of Hubble Space Telescope Images and Spectra”, in “*Deconvolution of Images and Spectra*”, Editor: P.A. Jansson, 2nd ed., Academic Press, CA, 1997.
10. T.K. Moon, “The Expectation-Maximization Algorithm”, *IEEE Signal Processing Magazine*, vol. 13, no.6, pp.47-60, Nov. 1996.
11. W. H. Richardson, “Bayesian-based Iterative Method of Image Restoration”, *J. Opt. Soc. Amer.*, vol. 62, pp. 55-59, 1972.
12. L. B. Lucy, “An Iterative Technique for the Rectification of Observed Distribution”, *Astronomical Journal*, vol. 79, pp. 745-754, 1974.
13. D.S.C., Biggs and M., Andrews, “Acceleration of Iterative Image Restoration Algorithms”, *Applied Optics*, vol. 36, no. 8, pp1766-1775, 1997.
14. T.J. Holmes, S. Bhattacharyya, J.C. Cooper, D.H. Hanzel, V. Krishnamurthi, W-C. L., B. Roysam, D.H. Szarowski and J.N. Turner, "Light Microscopic Images Reconstructed by Maximum Likelihood Deconvolution", in "*Handbook of Biological Confocal Microscopy*", Editor: J. B. Pawley, Plenum Press, New York, 1995.
15. X. H.-T. Pai, A. C. Bovik, and B. L. Evans, "Multi-Channel Blind Image Restoration", *TUBITAK Elektrik Journal of Electrical Engineering and Computer Sciences*, vol. 5, no. 1, pp. 79-97, Fall 1997.